Attenuation Artifacts in SPECT: Effect of Wrap-Around Lung in 180° Cardiac Studies

E.V.R. Di Bella, R.L. Eisner, A.B. Barclay, R.E. Patterson and D.J. Nowak

Department of Electrical Engineering, Georgia Institute of Technology; Departments of Medicine (Cardiology) and Radiology, Carlyle Fraser Heart Center, Crawford Long Hospital of Emory University, Atlanta, Georgia; and GE Medical Systems, Milwaukee, Wisconsin

We estimated that in 75%–90% of PET ^{82}Rb patients the left lung appeared to wrap around the anterior aspect of the left ventricle. We used clinical PET ^{82}Rb myocardial perfusion studies as the input to a SPECT computer simulation model to determine if patients with left lung wrap-around displayed consistent artifacts in reconstructed SPECT images. In particular, we sought an explanation for the hot lateral wall seen in SPECT images from normal female and male patients. **Methods:** Attenuated SPECT ^{201}Tl emission data were simulated from a mid-ventricular slice in 10 randomly selected clinical PET ^{82}Rb studies with left lung wrap-around. In these same cases, the influence of left lung wrap-around was removed by assigning the left lung an attenuation coefficient which matched that of the heart. Five randomly selected clinical PET ^{82}Rb studies without left lung wrap-around were also processed with our model. **Results:** In all 10 cases with left lung wrap-around, reconstructed SPECT images showed the hot lateral wall artifact with a mean septal-to-lateral wall count ratio of 0.86. With left lung wrap-around removed in the same 10 patients, reconstructed images did not show hot lateral wall (mean septal-to-lateral wall count ratio = 1.07). The 5 cases without left lung wrap-around did not show hot lateral wall (mean septal-to-lateral wall count ratio = 1.04) and the ratios changed little with the filling of the left lung (mean septal-to-lateral wall count ratio = 1.05). **Conclusion:** Results of our PET-to-SPECT computer simulation model showed that the hot lateral wall artifact found in SPECT myocardial perfusion images was related to the orientation and positions of the left ventricle and the left lung.

Key Words: myocardial perfusion imaging; SPECT; artifacts

J Nucl Med 1996; 37:1891–1896

Standard filtered backprojection (FBP) reconstructions of SPECT myocardial perfusion imaging studies suffer from widely variable attenuation effects. Breast tissue, adipose tissue, the liver and the diaphragm are highly variable attenuators capable of causing artifacts in SPECT images (*1–6*). However, SPECT ^{201}Tl myocardial perfusion images from normal patients show consistent inhomogeneities. For example, the inferior wall to anterior wall count ratio is close to unity for normal females, and is significantly less than one (0.86) for normal males (*2*). These gender-specific normal file patterns are related to differences in breast and diaphragmatic attenuation (*1,2*).

Another normal file pattern, represented by a decreased septal wall-to-lateral wall (SW/LW) count ratio, is found in both male (SW/LW = 0.86) and female (SW/LW = 0.89) stress SPECT ^{201}Tl normal files (*2*). To date, this hot lateral wall effect has not been definitively associated with an anatomical or physiological feature. To aid in understanding the underlying cause of the hot lateral wall effect, we used clinically acquired PET ^{82}Rb myocardial perfusion image data from our large (more than 1000) patient data base. We developed a methodology to simulate attenuated SPECT emission data from the clinical PET transmission and emission data. Our computer simulations using real patient data allowed us to extend the work of other researchers who used sophisticated mathematical models (*6,7*).

We hypothesized that, due to the relative importance of the projections tangential to the non-apical walls, differences in attenuation in selected views would result in a septal wall-to-lateral wall count ratio different from unity. Figure 1A shows an example in which the tangential rays which define the lateral wall of the left ventricle pass through less body tissue (though more lung) than the rays defining the septal wall of the left ventricle. For patients with this left lung wrap-around type of anatomy, we postulated that since the rays most important in defining the lateral wall pass through less attenuation than those rays defining the septal wall, the septal-to-lateral wall count ratio would be less than one. Figure 1B displays a case without left lung wrap-around. Here the lateral wall and the septal wall see similar amounts of attenuation in the most important (highest frequency or most perpendicular to the camera) views. Therefore, we hypothesized in these cases that the septal-to-lateral wall count ratio would be close to 1.0 and different from that in Figure 1A.

In this article, we used our PET-to-SPECT simulation to investigate this critical role of the relative heart/left lung orientation and position in defining attenuation artifacts. The PET-to-SPECT simulation enabled us to test our hypotheses with clinically-derived models.

METHODS

Initially, we generated projections at 64 angles over 180° from one slice of a uniform model of the left ventricle, without attenuation effects. A portion of the projection views was set to 0, to simulate a worst case of nonuniform attenuation. This was done to study the effect of a simple known attenuator on SPECT images of a heart-shaped structure. Five different sets of projection data were generated. Each had the projections in different angular ranges set to 0. The complements of these projection data sets were also reconstructed. That is, these images were reconstructed from projection angles where the data had been zeroed previously.

We then examined the reconstructed transmission scans from 167 PET ^{82}Rb patients. The criterion for left lung wrap-around was that rays tangential to the lateral wall had to traverse a significant part of the left lung in a mid-ventricular slice. The frequency of left lung wrap-around was estimated by two observers independently. Ten of the clinical PET ^{82}Rb studies (six men, four women) defined as having left lung wrap-around by both observers were chosen randomly to use with our computer simulation. Five studies (4 women, 1 man) without left lung wrap-around were selected at random for comparison.

Received April 26, 1995; revision accepted Oct. 8, 1995.

For correspondence or reprints contact: Robert L. Eisner, PhD, Carlyle Fraser Heart Center, Emory: Crawford Long Hospital, Department of Nuclear Cardiology, 550 Peachtree St., NE, Atlanta, GA 30365.

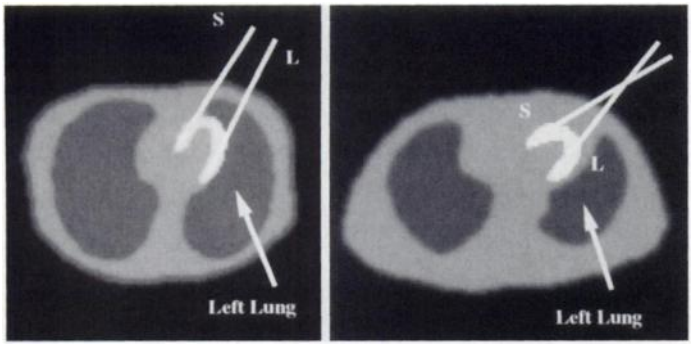

FIGURE 1. Thresholded myocardial PET emission image overlaid on the corresponding segmented PET transmission image. (A) Example of left lung wrap-around. Ray L which largely defines the lateral wall suffers less body attenuation than Ray S which largely defines the septal wall. (B) Example of a transaxial slice without left lung wrap-around. Ray L parallel to the lateral wall passes through a similar amount of attenuating tissue as Ray S parallel to the septal wall.

Synthetic Data Generation

Our computer simulation methodology used clinically-acquired PET ^{82}Rb emission and transmission data to construct myocardial and anatomical models suitable for use with a SPECT projector. The myocardial model was derived from smooth, filtered backprojection reconstructions of the PET emission data, corrected for attenuation. The PET reconstructions were resampled from 21 256 × 256 slices into 35 128 × 128 (3.1-mm isotropic voxels) slices. A mid-ventricular transaxial slice was then selected to use as the basis for a uniform count density model. A count threshold was chosen to give a uniform count density model that approximated the shape of the left ventricle in the reconstruction of the acquired data. Figures 2A and B display examples of the original PET filtered backprojection reconstructions. The corresponding resampled and segmented models for the emission and the transmission data are shown in Figures 2C and D. Patients were not used with defects such that the model of the left ventricle would not be representative of a normal myocardium. The system point response and scatter were not included when generating the projections in order to isolate attenuation effects. Using a rotation-based projector, SPECT projections were generated from the uniform model without attenuation, 64 views (128 bin) over a 180° right anterior oblique to left posterior oblique arc.

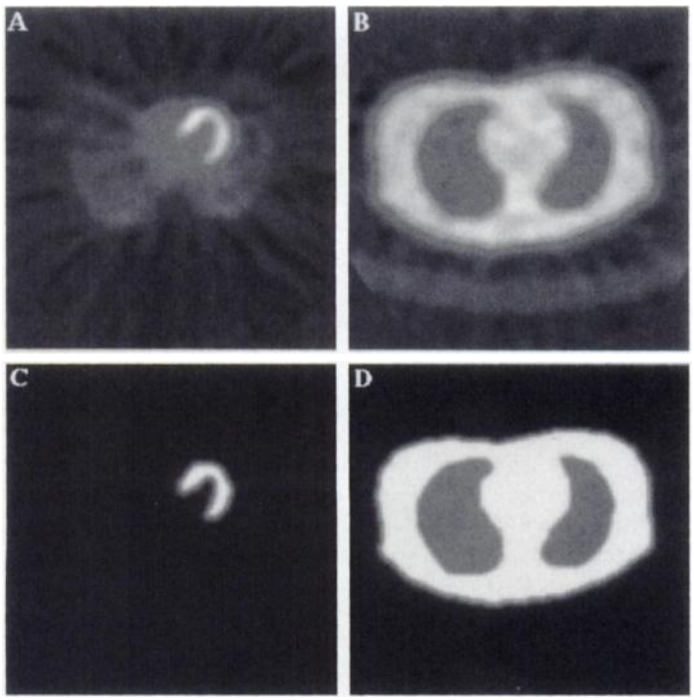

FIGURE 2. (A) Filtered backprojection reconstruction of PET transaxial slice. (B) Filtered backprojection reconstruction of corresponding PET transmission slice. (C) Resampled and segmented PET data corresponding to A. (D) Resampled and segmented PET data corresponding to B. Images C and D were used as models to generate SPECT projection data.

Two different attenuation models were created for use with the SPECT projector. For both models, a body outline was obtained from the patient's reconstructed transmission scan using a single threshold. The background was set to 0. The lungs were segmented with another threshold level. Attenuation coefficients appropriate for ^{201}Tl energies (tissue 0.18 cm^{-1} and lung 0.06 cm^{-1}) were assigned to each region to comprise the first attenuation model. The second attenuation model was identical except the left lung was assigned the same attenuation coefficient as tissue (0.18 cm^{-1}). After segmentation into lung, tissue and background, the transmission maps were smoothed with a two-dimensional Gaussian distribution function to reduce any aliasing effects.

A second set of SPECT ^{201}Tl projections was generated from the uniform model, but this time with the effects of attenuation from the first attenuation model. A third set of projections was generated similarly, but used the second attenuation map, that is, with the left lung assigned a value matching the tissue coefficient.

The three sets of projections—no attenuation, normal attenuation and attenuation map with the left lung filled—were generated for both the patients with left lung wrap-around and the patients without left lung wrap-around. In addition, a representative patient with left lung wrap-around and one without left lung wrap-around were chosen to demonstrate the effects of assigning the left lung a range of attenuation coefficients. A value of half the tissue attenuation coefficient and then a value of twice the tissue attenuation coefficient were assigned to the left lung.

Reconstruction

The images were reconstructed from the synthetic projections by filtered backprojection. The same filter used in our clinical SPECT studies, a Hanning filter with cutoff at half the Nyquist frequency, was employed.

Processing

Based around an operator-chosen center, a 64-ray maximum count circumferential profile was generated for each transaxial slice. Figure 3A shows the location of profile samples overlaid on a myocardial slice. Figure 3B displays the corresponding profile. The average maximum count in the septal wall region (approximately 1/5 of the slice, designated by S in Fig. 3A) and in a lateral wall region (L in Fig. 3B) was computed. SW is defined as the average of counts in Rays 10–20 and LW as the average of counts in Rays 40–50. No attenuation was modeled when generating the projections which were used to reconstruct the slice shown in Figure 3. The SW/LW count ratio is 0.99 for the slice.

Statistical Analysis

The mean and standard deviation of SW/LW were determined from each simulation set. Comparisons of differences between means were performed using a Student's t-test for paired or unpaired data, where appropriate. Differences were considered significant at the $p < 0.01$ level.

RESULTS

Zeroing Views

In filtered backprojection reconstruction, edges and other high frequencies are amplified according to the inverse Radon transform. Thus, rays tangential to structures contribute more significantly to the reconstruction. By zeroing certain projections before reconstruction, we can get an idea of the degree to

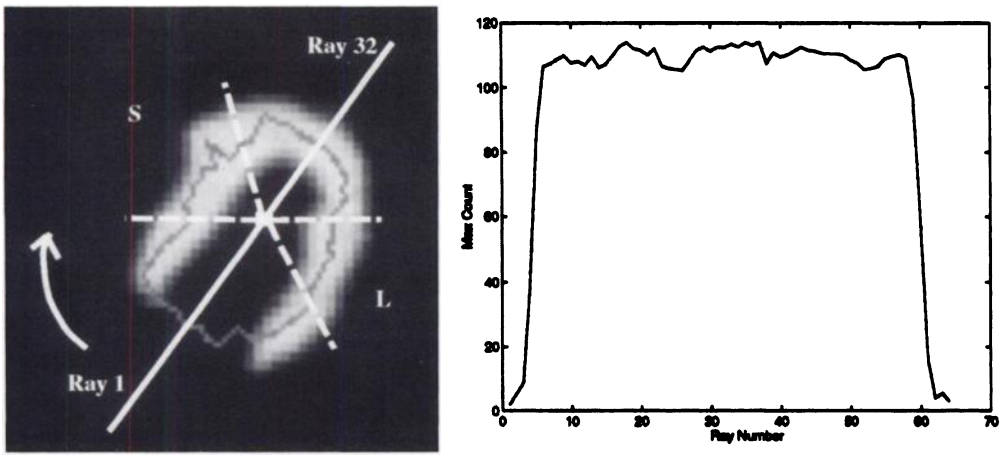

FIGURE 3. (Left) The gray line overlaid on the SPECT-reconstructed transaxial slice delineates the location of maximum count circumferential profile samples. (Right) Plot of maximum count circumferential profile curve corresponding to the left panel A. SW count is the average of counts in Rays 10–20; LW count is the average of counts in Rays 40–50. SW/LW = 0.99 in this example.

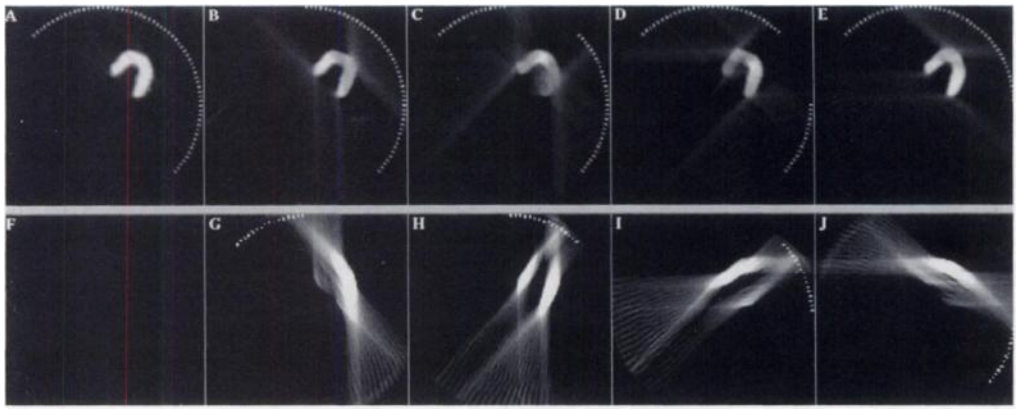

FIGURE 4. Filtered backprojection reconstructions from 64 views over 180°. In each image dots denote the positions of the camera center for every nonzero view. (A) Standard filtered backprojection reconstruction. (B) Views 1–16 set equal to zero. (C) Views 17–32 set equal to zero. (D) Views 33–48 set equal to zero. (E) Views 49–64 set equal to zero. (F–J) are the complements of (A–E), respectively. Note the effect on the structures perpendicular to the views which have been zeroed. Structures are reconstructed if they are perpendicular to the camera face at the views used to reconstruct the image.

which selected views contribute to the shape and structure of the reconstructed image. Setting projections to zero is analogous to complete attenuation of those views. Figure 4 demonstrates the result of completely attenuating, or zeroing, the views centered in the blank section of the arc. In all of the images (A–J) in Figure 4, each point in the arc represents the center of a camera face acquiring 128 parallel rays. Figure 4A shows a standard filtered backprojection reconstruction from simulated projection data at 64 views over 180°. In Figure 4B, the projection data in the first (beginning at the right anterior oblique position) 16 views were set equal to 0. In a like manner, the projection data were zeroed in views 16–32, 32–48 and 48–64, in Figures 4C–E, respectively. Note the effect on the structures perpendicular to the zeroed views. For example, the apex is considerably decreased by the omission of the side views (48–64) in Figure 4E. The complements of the images A–E in Figure 4 are shown in Figures 4F–J. Here, only the views zeroed previously are used to reconstruct the SPECT transaxial slice. As a result, only structures perpendicular to the camera face at the angles used obtain any structure. For example, as shown in Figure 4J, the side views (48–64) contribute mostly to the septal region near the apex. One can see that structures perpendicular to the camera face are defined by those views. All negative values were set to zero in these figures; the sums of the corresponding complements in Figures 4A–E and Figures 4F–J would give the standard filtered backprojection results if the negative values were retained.

Patients with Left Lung Wrap-around

The two observers estimated that 75%–90% of PET-reconstructed transmission images of the 167 randomly-selected patient PET ^{82}Rb studies showed the left lung wrapping around the front of the lateral wall in a mid-ventricular slice.

Mid-ventricular transaxial slice images overlaying the associated transmission scans from the 10 randomly-selected patients with left lung wrap-around are shown in Figure 5. The

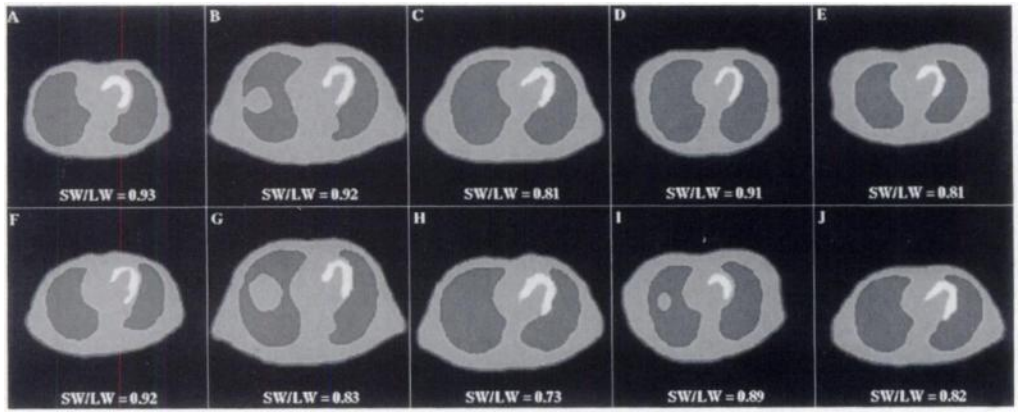

FIGURE 5. Transmission reconstruction overlaid by SPECT reconstruction of simulated projection data. All 10 patient images exhibit left lung-wrap around the anterior portion of the left ventricle. Due to left lung wrap-around, the projections defining the lateral wall typically pass through less attenuating media than the projections tangential to the septal wall. For each patient image, the SW/LW count ratio is shown. The average SW/LW ratio for these 10 patient images is 0.86 ± 0.06.

TABLE 1
SW-to-LW Ratios*

	No attenuation	Normal attenuation	Left lung filled
With lung wrap (n = 10)	1.00 ± 0.01	0.86 ± 0.06	1.07 ± 0.07†
Without lung wrap (n = 5)	0.99 ± 0.01	1.04 ± 0.08‡	1.05 ± 0.07§

*Mean ± s.d.
†$p < 0.01$ versus with lung wrap and normal attenuation.
‡$p < 0.01$ versus with lung wrap and normal attenuation.
§p = ns versus without lung wrap and normal attenuation.

figure depicts the segmented transmission data overlaid by the filtered backprojection reconstruction of nonattenuated simulated projection data. Envision, as in Figure 1, the path taken by rays tangential to the (nonapical) septal and lateral walls. The wrap-around of the left lung decreases the amount of attenuation encountered by some of the most important views. That is, the projections defining the lateral wall typically pass through less attenuation than the projections tangential to the septal wall, due to the left lung wrap-around. In all 10 cases with left lung wrap-around shown in Figure 5, the SW/LW count ratio is less than 1. The average SW/LW count ratio is 0.86 ± 0.06 (see Table 1). Assigning tissue values to the left lung results in more symmetric attenuation effects and an average SW/LW count ratio greater than 1.0 (1.07 ± 0.07, $p < 0.01$ versus unfilled; see Table 1). Note the wide variability in the body outlines of the patients shown in Figure 5.

Transaxial slice images from one patient with no attenuation, with normal attenuation and with the left lung filled with various tissue attenuation coefficients are shown in Figure 6. The top row displays images of the segmented attenuation coefficients overlaid by the associated filtered backprojection reconstruction and a representation of the acquisition arc. The filtered backprojection-reconstructed images are shown for each case in the bottom row. Figure 6F displays the result of filtered backprojection with no attenuation; Figure 6G is with normal attenuation; Figure 6H is with the attenuation values in the left lung increased to 0.5 times the body attenuation values; Figure 6I is with the left lung attenuation values equal to the body attenuation values; and Figure 6J is with the left lung attenuation values double the body attenuation values. These images show that there is a relative septal-to-lateral wall count increase as the left lung attenuation coefficient is increased.

The maximum count circumferential profiles from Figure 6F–J are shown in Figure 7. The curves have been normalized to the same count level in the septal wall region (between Rays 10–20). We see that SPECT reconstructions from unattenuated

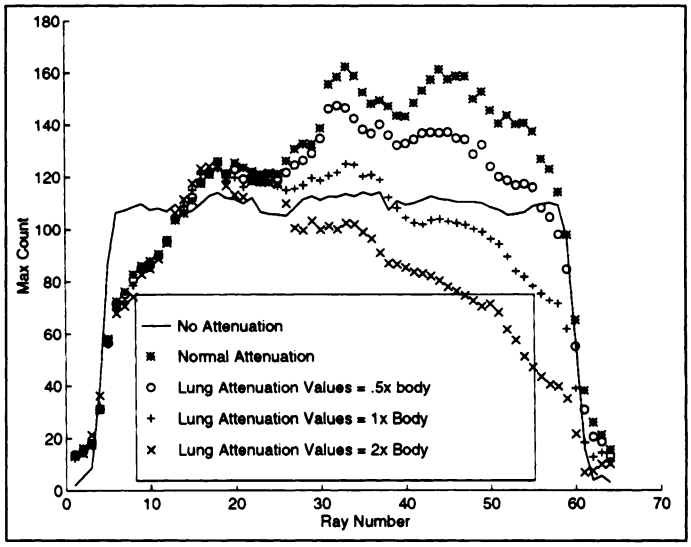

FIGURE 7. Maximum count circumferential profile curves from images shown in Figure 6. The profile curves have been normalized to the same count level in the septal region (Rays 10–20). The unattenuated projections result in a nearly constant profile. With normal attenuation coefficient values assigned to the body and lungs, counts in the lateral wall region are increased (* curve). Other profiles show the effect of increasing the value of the attenuation coefficients in the left lung. Septal-to-lateral wall count ratio increases as the left lung is assigned larger attenuation coefficient values.

projection data result in a nearly constant profile. Without compensation for attenuation effects, filtered backprojection reconstruction is not able to reconstruct the uniform myocardial activity distribution accurately. Thus, with normal attenuation values assigned to the body and lungs (Fig. 7), counts in the lateral wall region are increased. The other profiles show the effect of increasing the value of the left lung attenuation coefficient. The SW/LW count ratio is seen to increase as larger attenuation coefficient values are assigned to the left lung.

Patients without Left Lung Wrap-around

Mid-ventricular transaxial slices from the five randomly-selected patients without significant left lung wrap-around are displayed in Figure 8. These thorax anatomies are much less common in our PET patient population than those shown in Figure 5. The average SW/LW count ratio for this group (1.04 ± 0.08, Table 1) differs significantly from the group with the left lung wrap (0.86 ± 0.06; $p < 0.01$).

Figures 9A–J show a female patient without left lung wrap-around with no attenuation, with normal attenuation, with the attenuation values in the left lung increased to 0.5 times the body attenuation values, with the left lung attenuation values equal to the body attenuation values and with the left lung

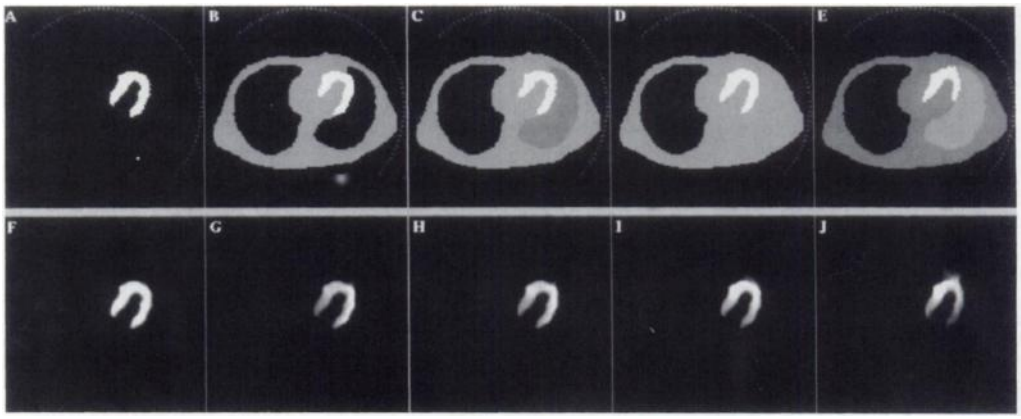

FIGURE 6. Representative patient data with left lungwrap. Top row: Overlay of transmission and emission data. Bottom row: Filtered backprojection reconstructed emission image. (A, F) Zero attenuation coefficients. (B, G) Normal attenuation coefficient values. (C, H) Attenuation coefficient values in the left lung increased to 0.5 times the body attenuation coefficient values. (D, I) Attenuation coefficient values in the left lung equal to the body attenuation coefficient values. (E, J) Attenuation coefficient values in the left lung set to double the body attenuation coefficient values. The septal-to-lateral wall count ratio increases as the left lung is assigned a higher attenuation coefficient value.

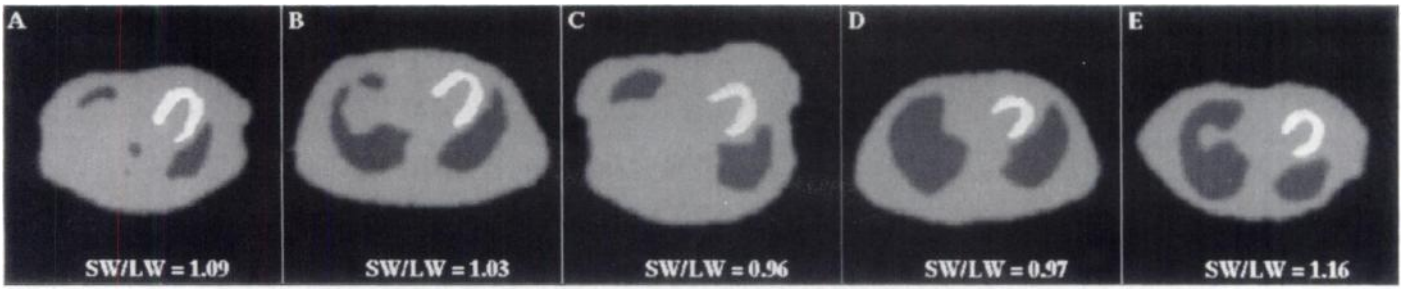

FIGURE 8. Transmission reconstruction overlaid by the reconstructed image of simulated projection data. All five images exhibit a lack of left lung wrap-around the anterior portion of the left ventricle. The projections most important in defining the septal and lateral walls typically pass through a similar amount of attenuating media. For each patient image, the SW/LW count ratio is shown. The average SW/LW ratio for these five patient images is 1.05 ± 0.07.

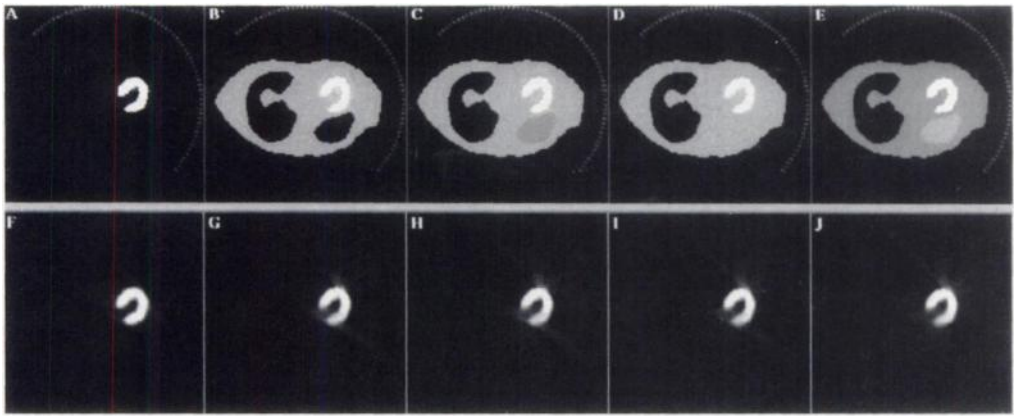

FIGURE 9. Representative patient data without left lung wrap. Top row: Overlay of transmission and emission data. Bottom row: Filtered backprojection reconstructed emission image. (A, F) Zero attenuation coefficients. (B, G) Normal attenuation coefficient values. (C, H) Attenuation coefficient values in the left lung increased to 0.5 times the body attenuation coefficient values. (D, I) Attenuation coefficient values in the left lung equal to the body attenuation coefficient values. (E, J) Attenuation coefficient values in the left lung set to double the body attenuation coefficient values. Septal-to-lateral wall count ratio remains nearly constant as the left lung is assigned a higher attenuation coefficient value.

attenuation values double the body attenuation values. In contrast to the results seen in Figure 6, filling the left lung makes little difference. The similarity between the circumferential profile curves displayed in Figure 10 demonstrates that the septal-to-lateral wall count ratio does not change as the left lung is assigned a higher attenuation coefficient in this patient without left lung wrap-around.

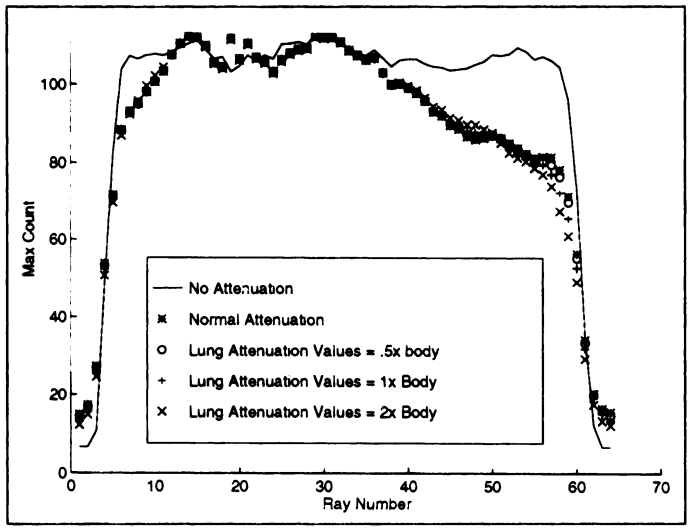

FIGURE 10. Maximum-count circumferential profile curves from images shown in Figure 9. The profile curves have been normalized to the same count level in the septal region (between Rays 10–20). With realistic attenuation coefficient values assigned to the body and lungs the septal-to-lateral wall count ratio is close to unity. Other profiles show the effect of increasing the value of the attenuation coefficients in the left lung. Septal-to-lateral wall count ratio changes little as the left lung is assigned larger attenuation coefficients.

DISCUSSION

The use of clinical PET myocardial perfusion imaging studies as cardiac models permits unique insights into attenuation effects in SPECT. With simple models and straightforward methodology, we have demonstrated a likely basis for the low SW/LW count ratios typical of SPECT normal files. Projections containing higher frequency components (below the cutoff of the reconstruction filter) contribute more significantly to reconstructed SPECT images. Accordingly, to understand and to predict the influence of the degrading effects of attenuation on SPECT images, it is important to do more than consider what structures are closest to significant attenuators, or even what structures are most attenuated. Rather, it is important to realize that the attenuation along the path of the rays that define structures is the most critical factor in determining the resulting attenuation artifacts. Thus, in general, our computer simulation model predicts a hot lateral wall in SPECT myocardial perfusion image slices when the tangential projection rays defining the lateral wall pass through the left lung while the tangential rays defining the septal wall pass through the heart and tissue.

The impact of the spatial relationship of the heart and the left lung on myocardial perfusion images is complex. In order to focus on major attenuation effects, several simplifications were made in this work. The degrading effects of the system point spread function and scatter were not modeled in our simulations. Also, the basal ends of the septal and lateral walls are typically high-frequency edges. The tangential rays defining the ends can have significant effects from lung attenuation. For this reason, the areas from which the septal wall and lateral wall count ratios were calculated were not at the extreme basal portion of the walls. Likewise, it is possible for the left lung to wrap around but not to produce the effect we describe. Other attenuators, such as the breast, may be in an abnormal position and overwhelm any other attenuation effects. Another situation is seen in Figure 8E,

where the left lung does not wrap, and the septal-to-lateral wall count ratio is greater than one. This case probably results from the significantly larger path that the rays most important in defining the lateral wall must pass through. Our results, however, have been remarkably consistent. All 10 patients with left lung wrap-around (Fig. 5) have a hot lateral wall.

Three-dimensional studies with all sources of degradation modeled will further contribute to our understanding of SPECT imaging artifacts. In our study, a single mid-ventricular slice was used in order to isolate the lung wrap-around effect. The anatomical relationship between lung and heart depends on the slice position. By our observations of many PET transmission and emission images, less left lung wrap-around is seen for more inferior transaxial slices. Therefore, we might expect the hot lateral wall artifact in SPECT normal files to be more pronounced in the anterolateral region compared to the inferolateral region.

CONCLUSION

This use of transmission and emission PET ^{82}Rb data to create attenuated SPECT ^{201}Tl patient data demonstrates that the left lung wrapping around the lateral wall of the left ventricle correlated with the increased counts in the lateral wall seen in SPECT files for normal men and women.

REFERENCES

1. DePuey EG, Garcia EV. Optimal specificity of thallium-201 SPECT through recognition of imaging artifacts. *J Nucl Med* 1989;30:441–449.
2. Eisner RL, Tamas MY, Cloninger K, et al. The normal SPECT thallium-201 bullseye display: gender differences. *J Nucl Med* 1988;29:1901–1909.
3. Manglos SH, Thomas FD, Hellwig BJ. Phantom study of breast tissue attenuation in myocardial imaging. *J Nucl Med* 1993;34:992–996.
4. Nowak DJ. Attenuation cause and effect relationships in cardiac SPECT imaging. In: *1st International Congress of Nuclear Cardiology*. Cannes, France: 1981.
5. Nuyts J, Dupont P, Van den Maegdenbergh V, et al. A study of the liver-heart artifact in emission tomography. *J Nucl Med* 1995;36:133–139.
6. Tsui BMW, Zhao XD, Gregoriou GK, et al. Quantitative cardiac SPECT reconstruction with reduced image degradation due to patient anatomy. *IEEE Trans Nucl Sci* 1994;41:2838–2844.
7. Zhao XD, Tsui BMW, Gregoriou GK, et al. Evaluation of corrective reconstruction methods using a 3D cardiac-torso phantom and bulls-eye plots. *IEEE Conference Record of the 1993 Nuclear Science Symposium and Medical Imaging Conference*. 1993; 2:1164–1168.

Automatic Preparation of Radiopharmacokinetic Data for In Vivo Estimation of Receptor Biochemistry

Jing Chun Xu, David R. Vera and Robert C. Stadalnik

Department of Radiology, University of California, Davis Medical Center, Sacramento, California

We present a fully automated region of interest (ROI) and motion correction program for the generation of heart and liver time-activity data resulting from a hepatic functional imaging study using [^{99m}Tc-]galactosyl-neoglycoalbumin (^{99m}Tc-NGA). **Methods:** The program automatically draws heart and liver ROI and corrects for lateral movement of the subject. Eighty-four ^{99m}Tc-NGA studies, consisting of 32 healthy subjects and 52 patients with liver disease, were processed and submitted to an automated kinetic analysis that estimates the subject's asialoglycoprotein receptor concentration $[R]_o$. **Results:** When compared to time-activity data generated by operator-drawn ROIs without motion correction, the average reduced Chi-square of the kinetic analysis decreased significantly ($p < 0.001$) from 2.20 to 1.37 and the number of studies that satisfied quality control increased from 74 to 81 studies. Receiver operating characteristic of $[R]_o$ resulted in greater detectability (0.984 ± 0.012 compared with 0.965 ± 0.020) when automatic ROI generation was employed. Using the test criteria of 0.65 μM, the sensitivity of $[R]_o$ increased from 0.88 to 0.92 and the specificity increased from 0.96 to 0.97. **Conclusion:** Automated definition of liver and heart ROIs with motion correction, that reduces observational noise, increased the success rate of the radiopharmacokinetic analysis from 88% to 96%.

Key Words: technetium-99m-NGA; kinetic modeling; automatic motion correction; automatic contour detection

J Nucl Med 1996; 37:1896–1902

Technetium-99m-galactosyl-neoglycoalbumin (^{99m}Tc-NGA) is a receptor-binding radiopharmaceutical (*1*) specific for the asialoglycoprotein receptor (ASGP-R) (*2*) that resides exclusively at the cellular membrane of hepatocytes. Consequently, a healthy liver will accumulate an excess of 90% of the dose within 15 min, whereas a diseased liver will accumulate significantly less activity during the same time period (*3*). In addition to high cellular specificity (*4*), another unique feature of ASGP-R is a lack of pharmacologic response to ligand binding. This feature enabled us to inject ^{99m}Tc-NGA in amounts that would occupy a significant fraction of ASGP-R. Consequently, we are able to operate the radiopharmacokinetic system as a bimolecular reaction (*5*), which permits high-precision measurements (*6*) of receptor concentration (*7,8*) from liver and heart time-activity data (*9*). Clinical studies have demonstrated that receptor concentration can differentiate (*10–13*) between healthy subjects and patients with liver disease. The largest study (*14*) reported to date, comprising 32 healthy volunteers and 52 patients, yielded a sensitivity of 88% for the detection of noncholestatic liver disease. The specificity was 96%.

Routine widespread clinical application of ^{99m}Tc-NGA pharmacokinetic modeling will require a fully automated analysis. One component of an automated analysis is the preparation of liver and heart time-activity curves, that provide the primary data for the pharmacokinetic analysis. This process requires two steps: (a) define the liver and heart regions of interest (ROIs) and (b) generate the time-activity curves by summing the counts within each ROI at every frame within the dynamic imaging study. Previous ^{99m}Tc-NGA functional imaging studies used standard nuclear medicine software with which the liver and heart ROIs were manually defined by lightpen and the time-activity curves were generated without correction for patient motion. Automation of this process would have two significant

Received May 26, 1995; revision accepted Jan. 28, 1996.

For correspondence or reprints contact: Robert C. Stadalnik, MD, Division of Nuclear Medicine, Research I Building, Rm. 1001, 4635 Second Ave., University of California, Davis, Medical Center, Sacramento, CA 95817.